energies

MDPI

Article

Modeling the Process and Properties of Ash Formation during Pulverized Biomass Combustion

Mingzi Xu and Changdong Sheng *

School of Energy and Environment, Southeast University, Nanjing 210096, China; 230169016@seu.edu.cn
* Correspondence: c.d.sheng@seu.edu.cn

Abstract: The present work mainly developed a mathematical model based on the plug flow model and coarse fly ash particles' fragmentation model to describe the behavior and evolution of ash formation and the influence of the biomass feeding rate and flue gas cooling rate on ash properties, which is validated by literature data. The model considers homogeneous nucleation of alkali vapors, heterogeneous condensation of vapors on newly formed particles and fly ash particles, and collision-coagulation between aerosol particles, which is also applied to numerically study and analyze the ash formation characteristics in the cases of practical boiler pulverized fuel combustion and SO_2 sulfation. The results show that the mathematical model can reasonably describe the ash formation and the influence of the biomass feeding rate and the flue gas cooling rate on the mass PSDs of PM_{10} and its elements. The initial nucleation temperature and initial nucleation particle size increase with the biomass feeding rate, which is of great importance to the cooling rate on the initial nucleation number concentration and the initial nucleation particle size. Elements Na, K, and Cl are mainly concentrated in PM_1, but rarely distributed in $PM_{1–10}$. The condensation of Na, K, and Cl on coarse particles increases with the biomass feeding rate and decreases with the cooling rate. The ash characteristics obtained from the experiment condition with an ultra-high flue gas cooling rate and minimum biomass selected may have a large deviation from that of practical biomass combustion, and the sulfated reaction may reduce Cl corrosion rather than ash deposition.

Keywords: pulverized biomass combustion; PSDs; ash formation; modeling; PM_{10}

Citation: Xu, M.; Sheng, C. Modeling the Process and Properties of Ash Formation during Pulverized Biomass Combustion. *Energies* **2022**, *15*, 4417. https://doi.org/10.3390/en15124417

Academic Editor: Mejdi Jeguirim

Received: 20 May 2022
Accepted: 15 June 2022
Published: 17 June 2022

1. Introduction

Biomass is regarded as renewable energy. It has great potential to be used as an alternative fuel for pulverized coal-fired power plants to mitigate CO_2 emission [1–3]. However, ash-related problems, including ash deposition [4] and consequent corrosion [1,5] of heat exchange surfaces, deactivation of the denitration catalyst [6–8], and particulate matter (PM) emissions [9–12], are among the major technical issues for applications of sole biomass combustion in existing power plants. The problems and their effects are significantly dependent on the properties of the ash formed during combustion processes. The ash deposition rate was found to be closely correlated with the concentration and composition of PM_1 (PM with an aerodynamic diameter of <1 μm) in the flue gas [13]. The deactivation of the denitration catalyst was proven to be associated with the deposition of alkali-containing aerosols [6,8]. The emission of PM_{10} (PM with an aerodynamic diameter of <10 μm) has serious environmental and human health implications [14] and, in particular, the emission of PM_1 is a major concern because of its low removal efficiency in air pollution control devices [15]. Therefore, properly describing ash formation is essential for understanding and managing ash-related problems during pulverized biomass combustion.

Pulverized biomass combustion generates inorganic PM or ash particles covering a wide range of sizes. The mechanisms of PM_1 and $PM_{1–10}$ are different. PM_1 [16,17] is mainly from volatiles' combustion, while $PM_{1–10}$ (PM with aerodynamic diameter of 1–10 μm) [18] is from char combustion and fragmentation during pulverized biomass combustion. The

condensation of alkali vapors and the deposition of particles also lead to changes in the composition and size of finer fly ash particles, which is one of the main characteristics of ash formation between pulverized biomass combustion and pulverized coal combustion. Therefore, it is an important part of describing the ash formation reflecting the formation and evolution of particulate matter during pulverized biomass combustion. The formation of PM_1 can be described in detail through a plug flow model to investigate the coupled processes of nucleation and condensation to predict submicron ash formation [19–22] or associated ash deposition [23]. The coarse fly ash can be described through the fragmentation model [23]. Due to the simultaneous or sequential transformation and interaction processes and the coupling effect between mechanisms, their contribution and influence on the formation and evolution of submicron particles and fly ash particles have not been fully understood. Therefore, further research is needed to describe the main processes and interactions of ash formation through the model approach, which is not only the basis for predicting the formation and evolution of ash formation [11,24], but also the basis for the evaluation of dust removal system performance and using additives to alleviate biomass ash-related problems during pulverized biomass combustion and co-combustion [11,24,25].

The previous models (pre-models), such as coarse fly ash formation, homogeneous nucleation, and sulfate reaction, were numerically studied [26–28], respectively. However, it is difficult for pre-models to describe the behavior and evolution of the size and composition of PM_{10} during biomass combustion. Therefore, the present work mainly developed a mathematical model based on the plug flow model and the coarse fly ash fragmentation model to describe the behavior and evolution of ash formation during pulverized biomass combustion, as shown in Figure 1. The main study areas are the properties and evolution of submicron particles and coarse fly ash particles and the influence of the biomass feeding rate and the flue gas cooling rate on ash properties such as mass concentration size distribution and yields of PM_{10} and its ash elements (Na, K, and Cl), which is validated by the experimental data in the literature [15]. Meanwhile, the model is also applied to numerically study and analyze the ash formation characteristics during practical boiler pulverized biomass (PF boiler) combustion and SO_2 sulfation.

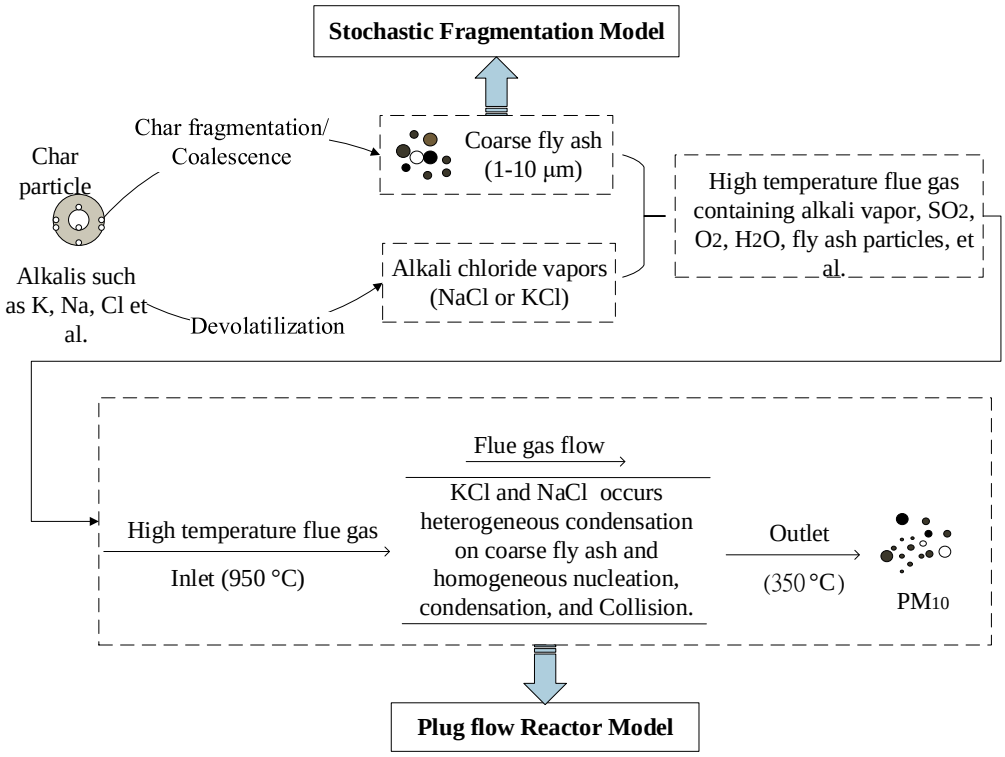

Figure 1. Main processes of ash formation during pulverized biomass combustion.

2. Modeling

During pulverized biomass combustion, the major part of the inorganic matter in the parent fuel transforms into residual fly ash, covering a wide range of particle sizes through fragmentation-coalescence mechanisms [28]. A small fraction releases into gas phase as the compounds containing alkalis, Cl, and S [20,29,30] during the combustion and transforms into submicron particles through gas–solid mechanisms or condenses on fly ash particles during the cooling of the flue gas. The main processes of ash formation are schematically shown in Figure 1. Considering the differences in the formation mechanisms, residual fly ash formation and gas–solid transformations are modeled separately. The former was assumed to proceed in flame with the burnout of fuel particles and was modeled with a fragmentation-coalescence model. The transformations of the vapors into ash particles were assumed to take place during the cooling process of the post-combustion flue gas and were described with a plug flow reactor model. The vapors transform into submicron ash particles via homogeneous nucleation, collision/coagulation, and heterogeneous condensation during the flue gas cooling. Meanwhile, the vapors condense on existing particles, and the submicron particles collide with fly ash particles, particularly the finer ones (mostly $PM_{1–10}$). Since a considerable fraction of the inorganic matter is volatile in the flame of pulverized biomass combustion, the vapor transformations lead to the evolutions of the size and composition of the submicron and finer fly ash particles [19,21] throughout the gas cooling, which are detailed in the modeling

2.1. Residual Fly Ash Formation Model

For pulverized biomass with a narrow size distribution (such as laboratory experimental fuel), a lognormal distribution can be approximately used to describe the particle size distribution (PSD) of the fuel as the input of the model, expressed as:

$$F(x) = \frac{1}{2}(1 + erf(-\frac{\ln(d_p) - \mu}{\sigma \cdot \sqrt{2}})) \quad (1)$$

where $F(x)$ is the percentage of the sieved mass with the size smaller than d_p (μm), μ is the logarithm of the average size (μm), and σ is the standard deviation to define the uniformity of the particle sizes. The smaller σ is, the narrower the PSD. It is worth noting that, due to the irregular shape of biomass particles, the sieve size, d_p, is generally the width, the smallest dimension, of the sieved particles [23]. However, as the model input, the volume-equivalent diameter was used in Equation (1) instead. It virtually lumps the effects of the size and shape of biomass particles on ash formation because their effects on the burning of biomass particles were not considered in the modeling.

It is assumed that, during the combustion of a biomass particle, a char particle breaks into several fragments and, after the burnout, forms spherical ash particles [31–33]. While the uniform breakage is too idealized to represent the residual ash formation, the fragmentation is likely to be a stochastic process. Therefore, a fuel particle is assumed to fragment randomly, and its fragmentation number follows a Poisson distribution [28]. The probability function is:

$$p(x) = \frac{(K_{mean})^k}{k!} \exp(-K_{mean}), k = 0, 1, 2 \ldots \quad (2)$$

where $p(k)$ is the probability of the breaking, $Kmean$ is the mean breaking number, and k is the fragmentation frequency, with $k = 0$ representing no fragmentation. With the number of the fragments determined, the mass of the ash particle is:

$$m_{ash} = m_{fuel} \cdot w_{ash}(1 - w_{vap})/(k + 1) \quad (3)$$

where m_{fuel} is the mass of the fuel particle, w_{ash} is the mass fraction of the ash in the particle, and w_{vap} represents the mass fraction of the ash released as the gases during the combustion. The size of ash particles can be calculated as:

$$d_{p,ash} = \sqrt[3]{\frac{\rho_{fuel} \cdot w_{ash}(1 - w_{vap})}{\rho_{ash} \cdot (k+1)}} \cdot d_p \tag{4}$$

The average numbers of fragments formed per particles during pulverized biomass combustion were observed to be above 3 [23]. In the present model, it is set as 5, that is, *Kmean* = 4, by fitting the PSDs of fly ash [15].

2.2. Model for the Evolution of the Aerosol

With the cooling of the flue gas, the vapors transforming into ash particles were described by a one-dimensional plug flow reactor model [19,21]. The model considered the processes of homogeneous nucleation, heterogeneous condensation, and coagulation between aerosol particles. Gas phase reactions of chlorides, i.e., sulfation, affect gas–solid transformations, and therefore ash formation and evolution. The effect can be considered [21,27,34], but not in the present model, which is focused on the effect of gas–solid transformations on the evolution of the aerosol PSD and the prediction of submicron ash composition.

Homogeneous nucleation was modeled based on the classical nucleation theory [35], which results from the increased concentration of the clusters to form stable nuclei, leading to homogeneous nucleation when the system becomes supersaturated. The nucleation rate is [21,27]:

$$J_{\text{hom}} = \left(\frac{2\sigma}{\pi M_i}\right)^{\frac{1}{2}} \frac{\nu {N_A}^2}{S} \exp\left(\frac{-16\pi}{3} \frac{\nu^2 \sigma^3}{(k_B T)^3 (\ln S)^2}\right) \tag{5}$$

where σ is the surface tension, M_i is molecular weight, v is the volume of the particle, N_A is the Avogadro constant, k_B is the Boltzmann constant, 1.3806×10^{-23} J/K, T is the temperature (K), and S is the saturation ratio, defined as:

$$S = \frac{P_i}{P_i^s(T)} \tag{6}$$

where ${P_i}^s$ is the saturated vapor pressure of matter i at temperature T.

The vapors also condense on existing particles in the system. The existing particles include newly formed particles by homogeneous nucleation and resulting particles from the processes of growth, such as coagulation, as well as residual fly ash particles. The condensation leads to not only the size growth but also the evolution of the particles' composition. At a certain saturation ratio, if the size of these particles exceeds the critical nucleation size of the vapor, heterogeneous condensation occurs. The condensation rate on a particle with a size of d_p is given as [21,27,36]:

$$J_c = \frac{2\pi d_{p,ex} D(P_i - P_i^e)}{k_B T} F(Kn) \tag{7}$$

with $d_{p,ex}$ representing the diameter of an existing particle (μm), D representing the gas molecular diffusivity, and ${P_i}^e$ representing the vapor pressure on the surface of the existing particle, which can be obtained from the Kelvin equation:

$$\ln\left(\frac{P_i^e}{P_{i\infty}}\right) = \frac{4\sigma M_i}{R_g T \rho_i d_p} \tag{8}$$

where $P_{i\infty}$ denotes the vapor pressure on an infinite plane. Since the sizes of the particles present in the aerosol system span from nanometers to micrometers, $F(Kn)$ used in

Equation (7) considers the diffusion over the range from the continuum to the free molecular regime, and expressed as a function of particle Knudsen number (Kn), given by [37]:

$$F(Kn) = \frac{1 + (\frac{2D}{d_p}\sqrt{\frac{\pi M_i}{8R_gT}})}{1 + 1.71\cdot(\frac{2D}{d_p}\sqrt{\frac{\pi M_i}{8R_gT}}) + \frac{0.667\pi M_i}{R_gT}(\frac{D}{d_p})^2} \quad (9)$$

In the flue gas system, heterogeneous condensation occurs simultaneously with homogeneous nucleation and competes for the vapors. Intensive condensation under certain conditions even depresses the nucleation.

Considering a huge number of particles in the aerosol system, the collision/coagulation occurs between the particles, and particularly between the finer particles because of their higher number density. The evolutions of the particle size, number, and composition are caused by coagulation. Assuming that the particle collision is bi-directional, and the collided pair coagulates to form a spherical particle, the particle number changing with time can be described by the classical Smoluchowski equation, written in a discrete form as [38]:

$$\frac{\partial n_k}{\partial t} = \frac{1}{2}\sum_{i=1}^{k-1}\beta_{i,k-1}n_i n_{k-i} - n_k\sum_{i=1}^{\infty}\beta_{i,k}n_i \quad (10)$$

with n_k denoting the number concentration of k-fraction particles in the system, and $\beta_{i,k}$ representing the collision rate of the particle pair i and k, also known as the kernel function depending on the collision mechanism. The collisions between fine particles are dominant in the simulated aerosol system, where Brownian motion plays a key role [21,39], and its kernel function is [38]:

$$\beta^B_{k,i} = \frac{2k_BT}{3\mu}(v_k^{\frac{1}{3}} + v_i^{\frac{1}{3}})(C_k v_k^{-\frac{1}{3}} + C_i v_i^{-\frac{1}{3}}) \quad (11)$$

with v_i and v_k representing the volumes of particles i and k, respectively, μ representing the viscosity of the flue gas, and C_i and C_k denoting the Cunningham factors of particles i and k, respectively, which are related to the Knudsen number:

$$C = 1 + Kn(a_1 + a_2\exp(-a_3/Kn)) \quad (12)$$

where a_1, a_2, and a_3 are constants [38], with the corresponding values of 1.142, 0.558, and 0.999, respectively. Other processes, including the turbulence and diffusion, leading to the coagulation can also be considered [20], provided that their kernel function is included. The coagulation process of the aerosol system was simulated by employing a discrete MC (Monte Carlo) numerical method [26], which facilitates tracking the changes in the particle number, size, and composition due to the coagulation as well as condensation. Therefore, the model is enabled to represent the evolutions of ash particles.

2.3. Model for the Evolution of the Aerosol

In the present model, the actual flue gas generated by the combustion of biomass is determined according to the composition supply rate of the fuel and the air supply rate [15]. The concentration of alkali vapor (KCl or NaCl) in flue gas is obtained by calculating the ratio of alkali vapor to the actual flue gas. We assumed that all K or Na will combine with Cl in the form of ACl (A represents Na or K) [15]. Due to their similar physical properties, an equal mole of Na was represented by K to simplify the model calculation [15]. The model inlet and outlet temperature are 950 °C and 350 °C, respectively, according to the literature [15]. The formation characteristics of PM_{10} and its main ash elements at the outlet of the reactor, such as mass concentration size distribution and yield, were mainly obtained. The biomass used in the experiment [15] has high alkali and chlorine contents but an extremely low sulfur content. The produced submicron ash particles are dominated by the chlorides [29,40], which enables the model to clarify the gas–solid transformation of

alkali chlorides and its influence on the aerosol evolution, while avoiding describing the complex effects of the sulfation of the chlorides on the gas–solid transformation and ash formation in the modeling.

The model was validated with the experiments of Liaw and Wu [15], in which wood bark particles with a narrow size of 150–250 μm were burned at 1300 °C in air in a drop tube furnace with well-controlled reaction conditions. The produced PM_{10} was collected by a low-pressure impactor and analyzed for the particle size and elemental composition. Moreover, the experiments were conducted at two different fuel feeding rates and four different cooling rates, which allow the model validation of the effects of vapor and fly ash particle concentration and the flue gas cooling rate on the submicron ash formation and the evolution of the aerosol properties.

3. Results and Discussion

Considering the narrowly sized biomass particles (150–250 μm) fed in the experiments, a log-normal distribution with the parameters of u = 2 and σ = 0.28 was used to fit the PSD of the fuel particles as the model input. Assuming fly ash formation based on the stochastic fragmentation model and the fitted fragmenting number of *Kmean* = 4 is used, the model can well-represent the PSDs of coarse ash particles, i.e., $PM_{1–10}$ formed in all experimental cases. Considering that the sizes of larger ash particles are hardly affected by the vapor condensation and particle coagulation, the PSD of fuel particles and the fitted fragment number were fixed for the fragmentation model to predict the PSD of the residual ash particles generated from the combustion of biomass particles. The calculated number and mass PSDs of residual fly ash particles are shown in Figure 2, assuming that the particles were broken stochastically. As can be seen, the coarse fly ash particles, containing a small mass but a dominant number, with diameter smaller than 2 μm, may be accessible for the vapor condensation and fine particle deposition through collision.

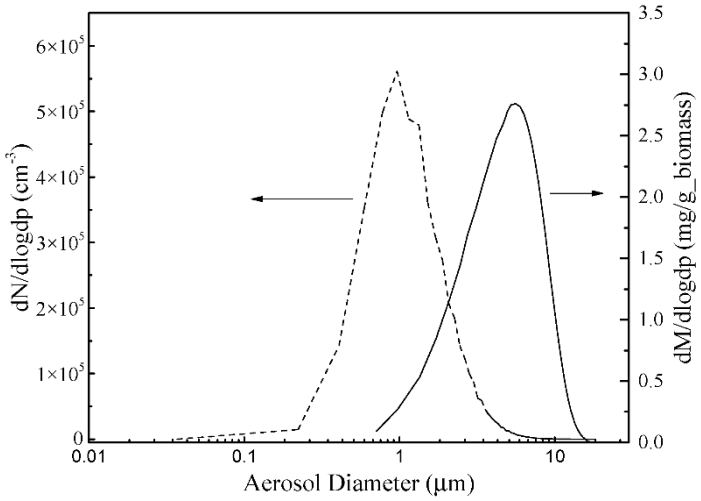

Figure 2. The Mass and number particle size distributions of the fly ash particles are from pulverized biomass combustion, assuming the stochastic fragmentation model.

3.1. Model Validation of the PSDs of PM_{10} and Its Elements

Figure 3 is the comparison of the mass-based PSDs of PM_{10} calculated by the model at different cooling rates with the experimental measurements [15] at the biomass feeding rate of 0.25 g/min. It can be seen that, in general, the model can well-reproduce the bimodal PSDs of PM_{10}. The model can also predict that the fine-mode diameter gradually moves to the large size direction, the peak width becomes narrower, but the peak concentration increases slightly with the decrease of the cooling rate. For example, with the decrease of the cooling rate from 20,000 to 1000 °C, the peak diameter of fine mode predicted by the model decreased from 0.077 to 0.042 μm, while the measured value decreased from 0.079 to

0.042 μm. The model reflects that the nucleated particles are larger in size but smaller in number at the lower cooling rate. Since a lower cooling rate means a long residence time at a higher temperature, heterogeneous condensation and collision lead to greater growth of submicron particles. The collision can also generate a small amount of relatively larger particles, resulting in a wide distribution of submicron particles.

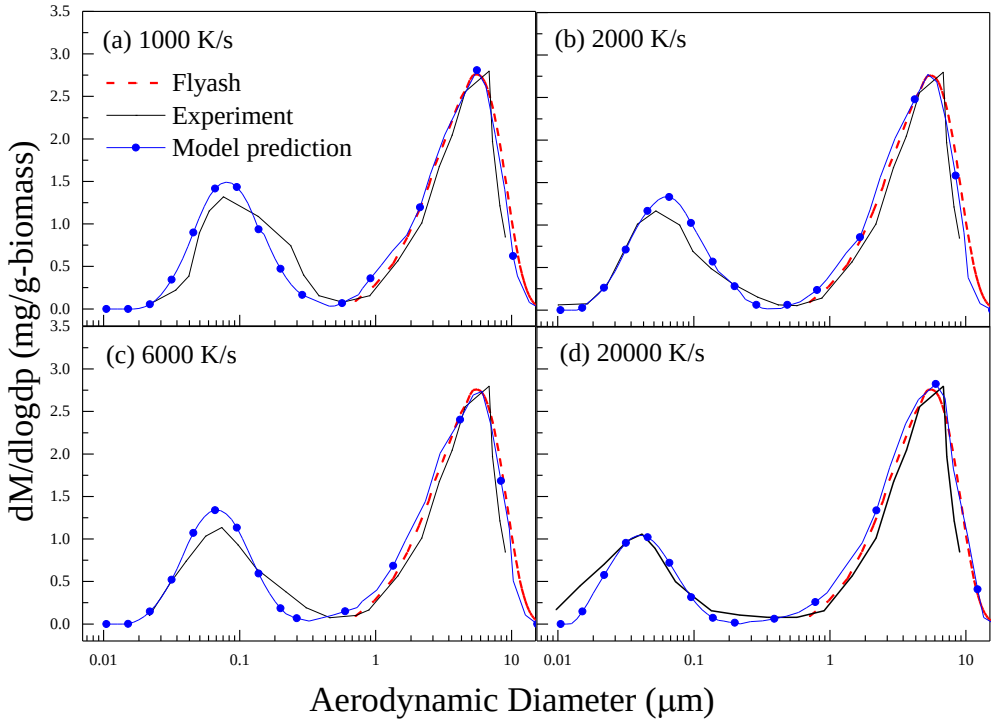

Figure 3. The calculated PSDs of PM_{10} formed at four different cooling rates (1000, 2000, 6000, and 20,000 °C) at a biomass feeding rate of 0.25 g/min compared with the measurements [15].

The mass-based PSD of fine-mode particles calculated by the model and its variation with the cooling rate were also roughly consistent with the experimental results at the biomass feeding rate of 0.05 g/min (not shown here).

Figure 4 shows that the calculated PSDs of inorganic elements in PM_{10} with the cooling rate being 1000 and 2000 °C/s were compared with the measurements and the calculated condensation amounts of elements on coarse fly ash particles at the biomass feeding rate of 0.05 g/min. As can be seen, the calculated element mass PSDs were basically consistent with the measurements in the fine-mode PSDs. The model can also well-predict that with the decrease of the cooling rate, the fine-mode PSDs of elements (Na/K/Cl) gradually moved to the large size direction, the peak width became narrow, but the peak concentration slightly increased, which is consistent with the fine-mode PSDs of PM_{10}. It is worth noting that the mass PSDs of Cl measured in the experiment had a small peak in the range of 1–10 μm, while the calculated PSD of Cl did not contain this peak. The model calculation only considers the heterogeneous condensation of alkali chlorine gas on the coarse fly ash particles of 1–10 μm and ignores the combination of Ca and Mg with Cl, which can affect the PSDs of Cl. However, the model can reasonably describe the influence of the flue gas cooling rate on the mass and PSDs of elements' (Na/K/Cl) fine-mode particles. It also shows that the mass PSDs of Cl in $PM_{1–10}$ may be underestimated if only considering the deposition of alkali chlorine gas on coarse fly ash particles, which is also the direction of subsequent model improvement. The mass PSDs of fine-mode particles calculated by the model and their variation with the cooling rate are also in good agreement with the experimental results at the biomass feeding rate of 0.25 g/min, as shown in Figure 5.

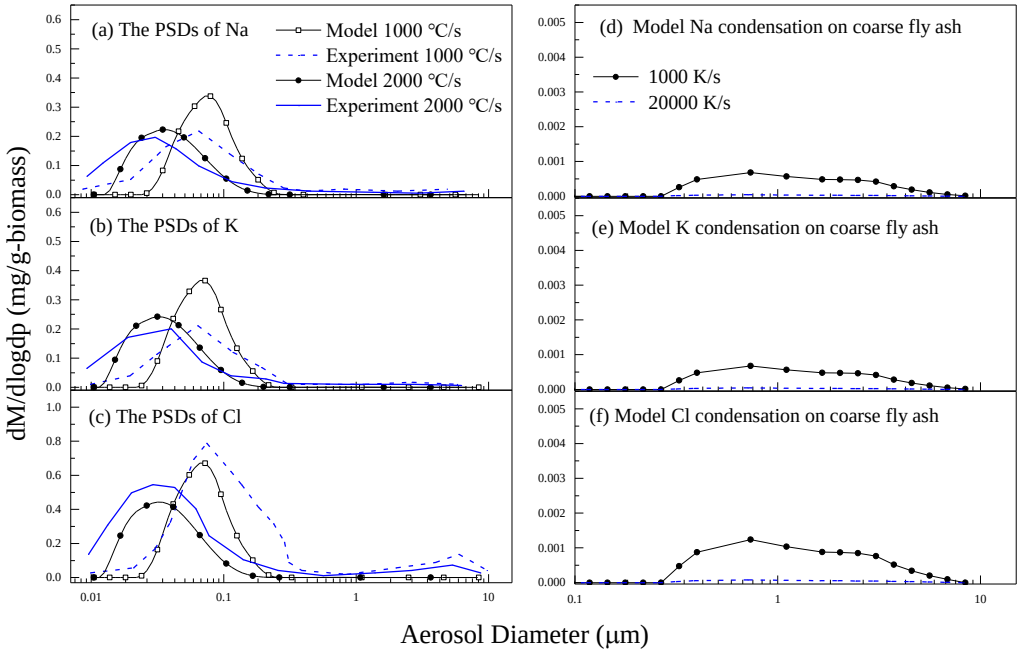

Figure 4. When the cooling rate is 1000 and 2000 °C/s, the calculated mass PSDs of inorganic elements in PM_{10} are compared with the measurements and the calculated condensation amount of the elements on coarse fly ash particles at the biomass feeding rate of 0.05 g/min, where (**a**–**c**) are PSDs of PM_{10}. (**d**–**f**) Condensation of elements on fly ash particles.

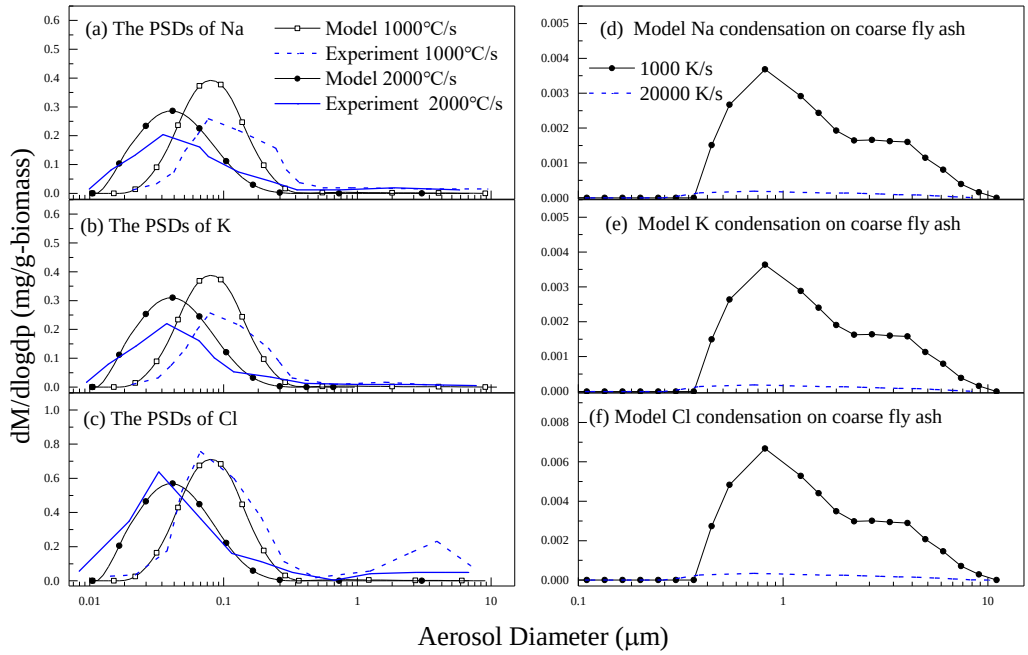

Figure 5. When the cooling rate is 1000 and 2000 °C/s, the calculated mass PSDs of inorganic elements in PM_{10} are compared with the measurements and the calculated condensation amount of the elements on coarse fly ash particles at the biomass feeding rate of 0.25 g/min, where (**a**–**c**) are PSDs of PM_{10}. (**d**–**f**) Condensation of elements on fly ash particles.

Figure 4d–f show the heterogeneous condensation of elements Na, K, and Cl in the particle size range of 1–10 μm. As can be seen, with the increase of the cooling rate, the condensation amounts of elements on existing particles increased, e.g., for Na, the condensation amount on coarse fly ash particles within 1–10 μm, with the cooling rate being 1000 °C/s, was much higher than that at 20,000 °C/s, indicating that heterogeneous

condensation occurs much more on submicron particles and less on coarse fly ash at lower cooling rates. Since the residence time of flue gas in high-temperature regions is longer at a lower cooling rate, heterogeneous condensation and collision condensation mechanisms lead to the evolution and growth of submicron particles. Compared with Figures 4 and 5, the condensation amounts of elements on particles within 1–10 μm increased significantly with the increase of the biomass feeding rate, because a higher biomass feeding rate can produce higher vapor pressure, which can promote a much higher number of new fine particles through homogeneous nucleation, and these elements will produce much more condensation on coarse fly ash particles. It can be seen that the biomass feeding rate or ash components significantly affect the heterogeneous condensation of elements on fly ash particles.

3.2. The Properties of PM_{10} and Its Elements

Table 1 shows that the model calculated the initial nucleation number concentration, initial nucleation particle size, nucleation temperature, and initial nucleation rate of alkali chlorine gas, which varied with cooling rates at two different cooling rates. The initial nucleation temperature, the initial nucleation size, and the number increased with the biomass feeding rate, indicating that the homogeneous nucleation can be strengthened with a higher biomass feeding rate, e.g., the nucleation temperature was about 650 °C with a biomass feeding rate of 0.25 g/min, which is much higher than 596 °C at 0.05 g/min. The higher biomass feeding rate will produce a higher alkali vapor concentration, which can reach super-saturation at a higher flue gas temperature and result in homogeneous nucleation, as a result of producing much higher numbers of submicron particles. However, with the increase of the cooling rate from 1000 to 20,000 °C/s, the homogeneous nucleation temperature decreased from 652 to 646 °C and the initial nucleation number concentration increased from 5.87×10^7 to 32.9×10^7 cm^{-3}, but its size decreased from 75.2 to 43.4 nm at a biomass feeding rate of 0.25 g/min, which indicated that a higher cooling rate would promote more but smaller particles. Since a higher cooling rate means a shorter residence time, the collision probability between particles was reduced, which is not favorable to the growth of new nucleation particles.

Table 1. The model calculated the initial nucleation number concentration, initial nucleation particle size, nucleation temperature, and initial nucleation rate of alkali chlorine gas, varying with cooling rates at two different cooling rates.

Biomass Feeding Rates /g min^{-1}	Cooling Rate /°C·s^{-1}	Initial Nuclei Number Concentration/10^7 cm^{-3}	Initial Nuclei Size/nm	Nucleation Temperature /°C
0.05	1000	2.6	59.7	596
	2000	6.18	45.1	594
	6000	6.21	45.2	593
	20,000	21.8	30.3	588
0.25	1000	5.87	75.2	652
	2000	8.96	65.9	650
	6000	17.9	52.4	650
	20,000	32.9	43.4	646

Figure 6a shows that the calculated peak diameter varied with the cooling rate at two biomass feeding rates. It can be seen that the fine-mode diameter decreased with the increase of the cooling rate, because the lower cooling rate means a longer residence time, which can increase the heterogeneous condensation and promote the growth of nuclei. The fine-mode diameter decreased from 0.066 to 0.0316 μm as the cooling rate increased from 1000 to 20,000 °C/s at a biomass feeding rate of 0.05 g/min, indicating that the cooling rate has an important influence on the characteristics of submicron particles. Meanwhile, the coarse-mode diameters under the two biomass feeding rates were almost unchanged (as shown in Figure 6). The formation of coarse fly ash particles is based on

the "fragmentation-coalescence" mechanism, which is only related to the PSDs of fuel, density, and the fragmentation number of fuel particles, but not related to the cooling rate of flue gas. It can be seen that the flue gas cooling rate mainly affects the submicron particles generated by homogeneous nucleation, heterogeneous condensation, collision condensation, and other mechanisms based on the decrease of the flue gas temperature. It can also be seen that at the same cooling rate, the 'fine-mode' diameter and 'coarse-mode' diameter at a biomass feeding rate of 0.25 g/min were above 0.05 g/min, indicating that when the biomass feeding rate is large, the formed ash particle size is large, which is consistent with the previous conclusions. Therefore, in the practical pulverized biomass combustion, controlling the biomass feeding rate is of great significance for the emission of fine particles.

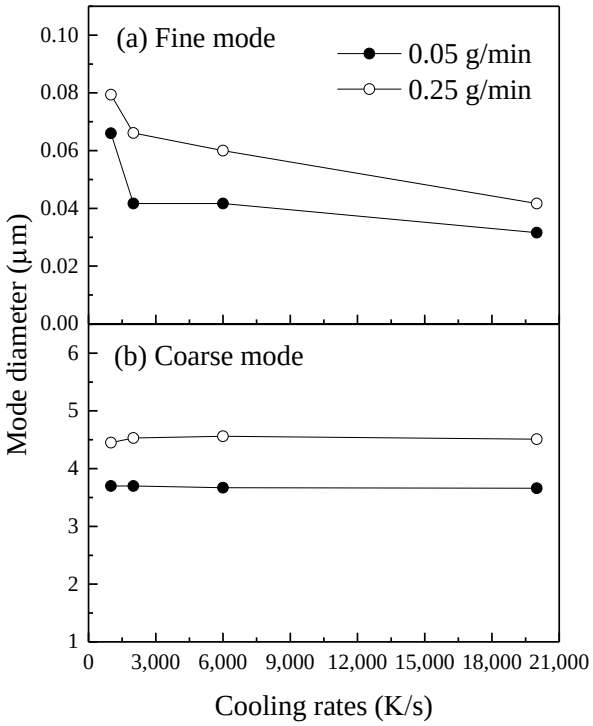

Figure 6. The calculated peak diameter varies with cooling rate at two biomass feeding rates. (**a**) Fine modal diameter and (**b**) coarse modal diameter.

Figure 7 is a comparison between the calculated and experimental yields of PM_{10} at different cooling rates under two biomass feed rates. It can be seen that with the increase of the cooling rate, the calculated yield of $PM_{0.1}$ increased, and the yield of $PM_{1–10}$ had little change (about 0.7 and 1.0 mg/g, respectively), which is consistent with the trends of measurements, indicating that the model can predict the yield of PM_{10}. With the increase of the cooling rate, as shown in Figure 7a, the yield of $PM_{0.1}$ increased and the yield of $PM_{0.1–1}$ decreased, leading to the unchanged yield of PM_1, about 0.68 mg/g, which means that a higher cooling rate can promote homogeneous nucleation and generate more $PM_{0.1}$. Since the formation of $PM_{1–10}$ is mainly based on the 'fragmentation-coalescence' mechanism, its yield is almost unaffected by the cooling rate. It can also be found that the calculated yield of PM_1 was almost not affected by the biomass feeding rate (0.67 mg/g), but the yield of $PM_{1–10}$ increased with the biomass feeding rate, which is different from the experimental measurement with the yield of $PM_{1–10}$ being not affected by the biomass feeding rate. The deviation of $PM_{1–10}$ yield between the model and experiment is maybe because the model calculation only considers the alkali chloride vapors and neglects the influence of Mg and Ca.

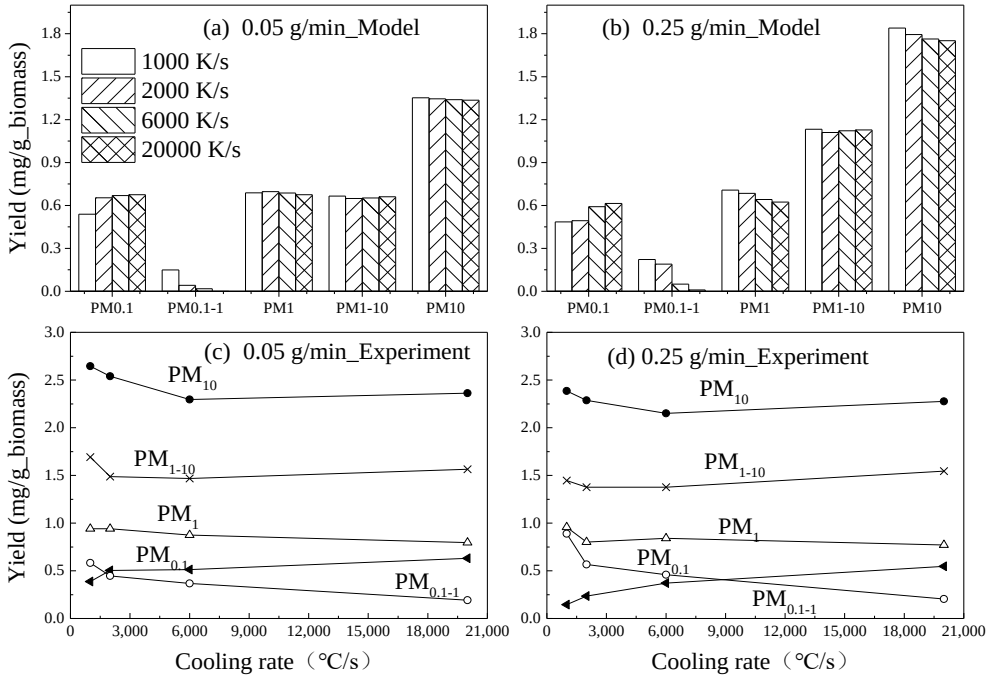

Figure 7. The comparison of the calculated yields of PM_{10} with experimental measurements varies with different cooling rates at two biomass feeding rates. (**a**,**b**) are the calculated yields of PM at the biomass feeding rate of 0.05 g/min and 0.25 g/min, respectively; (**c**,**d**) are the measured yields of PM at the biomass feeding rate of 0.05 g/min and 0.25 g/min.

With the increase of the cooling rate, the calculated yield of Na (or K or Cl) in $PM_{0.1}$ increased, the yield of $PM_{0.1–1}$ decreased, and the total yield of PM_1 remained unchanged (~0.178 and ~0.172 mg/g). The calculated yield of PM_{10} was almost unchanged, indicating that the condensation amounts of elements (Na, K, Cl) on the coarse fly ash particles were too small to influence the total yield of PM_{10}. It can be seen that the calculated condensation amounts of elements (Na, K, Cl) on the coarse particles within 1–10 μm increased with the biomass feeding rate, which is consistent with Figures 4 and 5; that is, a higher biomass feeding rate leads to higher condensation amounts of elements on coarse fly ash particles. The higher biomass feeding rate promotes the higher vapor concentrations of alkali vapors in flue gas, thereby increasing their condensation on coarse particles. As can be seen in Figure 8, the condensation of elements (Na, K, Cl) on coarse particles decreases with the cooling rate because the flue gas residence time is too short for alkali chlorine vapors to be fully condensed on coarse particles at a higher cooling rate (e.g., 20,000 °C/s). At a lower cooling rate (e.g., 1000 °C/s), alkali vapors have a longer condensation time.

It can be seen that the cooling rate and biomass feeding rate have an important influence on the mass PSDs and the yield of PM_{10} and its elements, which is manifested in the change of fine-mode mass PSDs with the cooling rate, and the high biomass feeding rate will significantly affect the characteristics of ultrafine ash particles (1–10 μm). The model can be used to predict the yields of PM_{10} and its elements, as well as the condensation of Na, K, and Cl on 1–10 μm particles.

Above all, the calculated results in Figures 3–8 provide direct evidence to demonstrate the significant effect of the flue gas cooling rate and the biomass feeding rate on the properties (e.g., overall and elemental PSD and yields) of PM_1 and PM_{10}. Heterogeneous condensation can take place at a super-saturation ratio (SR) of slightly >1, however, homogenous nucleation only takes place at a higher SR, typically at 2–10 [19]. A high flue gas cooling rate (20,000 °C/s) favors the homogenous condensation process, and the nucleation rate is much higher. A higher cooling rate, such as 20,000 °C/s, means a shorter the residence time, which is too short for inorganic vapors to condense on coarse fly ash particles, as a result of a lower condensation amount on $PM_{1–10}$ (shown in Figures 4, 5 and 8).

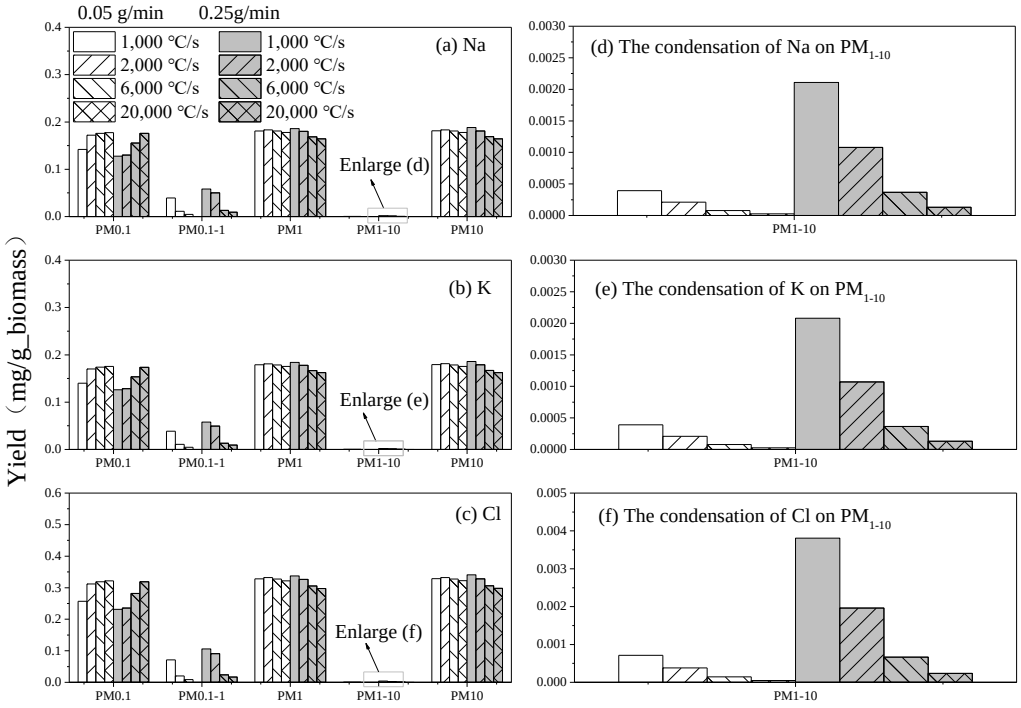

Figure 8. The yield of elements in PM_{10} and the condensation amounts on $PM_{1–10}$ at different cooling rates were calculated under two biomass feeding rates. (**a**–**c**) are the calculated yields of elements Na, K and Cl, respectively; (**d**–**f**) are the condensation of elements Na, K and Cl on $PM_{1–10}$, respectively.

3.3. Further Numerical Research

The above model study is based on the experimental conditions in the literature [15], which is carried out under the condition of a much higher air–fuel ratio (the ratio of air and fuel feeding rate) and cooling rate than the actual suspension boiler combustion. In this study [15], after calculation, the air–fuel ratios were 25 and 5, respectively, and the air feeding rate was 5.6 L/min, corresponding to the two biomass feeding rates being 0.05 and 0.25 g/min. However, the air–fuel ratio of the practical boiler pulverized biomass (PF boiler) combustion was generally about 1.2. Meanwhile, the flue gas cooling rates were all above 1000 °C/s in the experiment [15], which was used to check the mathematical model, while the practical flue gas cooling rate was 300–600 °C/s. A higher cooling rate may underestimate the heterogeneous condensation of alkali vapor on fly ash particles or overestimate the homogeneous nucleation of alkali vapor. To study the PM_{10} characteristics generated from pulverized biomass during practical PF boiler combustion, the air–fuel ratio was set as about 1.25 and the flue gas cooling rate was 400 °C/s (within the range of the flue gas temperature cooling rate in the super-heater area of the typical biomass combustion boiler). In this case, the biomass feeding rate was about 1 g/min, which was called the "practical PF boiler combustion". The influence of a small amount of sulfate reaction in flue gas is not considered in the model calculation. Therefore, an "adding SO_2" case was introduced to study the effect of sulfur (S) on ash formation during combustion in this model. During this case, 50 ppm SO_2, 5% H_2O, and 5% O_2 were added to the flue gas at a 0.05 g/min biomass feeding rate (the details about sulfation can be found in our previous work [26]), and the flue gas cooling rate was 1000 °C/s. At the same time, the "reference case" was also considered. During calculation, the inlet and outlet temperatures of the model reactor were also 950 and 350 °C, respectively. The three cases in this model are as follows:

(1) Practical PF boiler combustion case: air–fuel ratio is about 1.25, cooling rate is 400 °C/s.
(2) Adding SO_2 case: biomass feeding rate is 0.05 g/min and cooling rate is 1000 °C/s, adding 50 ppm SO_2, 5% H_2O, and 5% O_2 to flue gas.

(3) Reference case: biomass feeding rate is 0.05 g/min and cooling rate is 1000 °C/s.

Figure 9 shows the comparison of calculated mass PSDs of PM_{10} particles in the three different cases. As can be seen, the mass PSDs of PM_{10} had bimodal distribution in the three cases. Compared with the reference case, the mass PSD of PM_{10} calculated by the actual PF boiler combustion case moves to the right, which indicates that the fine-mode diameter calculated under the PF biomass combustion case is relatively large, because the slow cooling rate is conducive to the collision of newly generated particles and is also favorable to the heterogeneous condensation of alkali vapor on newly generated particles, which promotes the growth and evolution of submicron particles. Moreover, there is a 'shoulder peak' that appears near 1 μm, which is due to the collision/aggregation of submicron particles with finer fly ash particles and the heterogeneous condensation of alkali chlorine vapor on finer fly ash particles. It means that the formation of intermediate-mode particles is not only related to the finer breaking of fly ash particles but also the interaction of submicron generation. The significant difference between the predicted results of the "practical PF boiler combustion case" and the "reference case" means that the ash characteristics of biomass combustion under experiment conditions with an ultra-high flue gas cooling rate and a lower biomass feeding rate may deviate from the practical ash characteristics after pulverized biomass combustion.

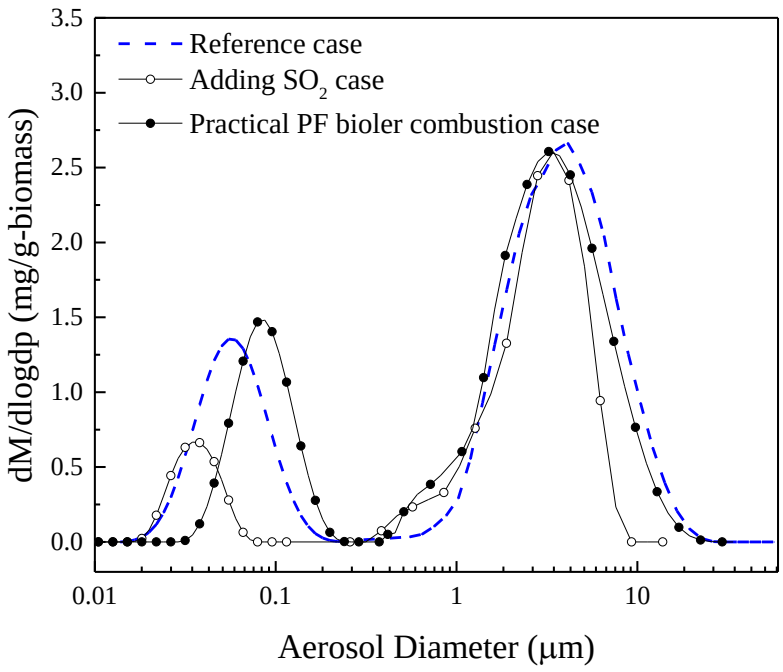

Figure 9. The comparison of calculated mass PSDs of PM_{10} particles in the practical PF boiler combustion case, adding SO_2 case, and reference case. At 800–1100 °C, KCl vapor is converted to K_2SO_4 vapor through a global reaction [26,34]: $KCl + H_2O + SO_2 + 1/2O_2 \rightarrow K_2SO_4 + 2HCl$. The pre-exponential factor of the rate constant of SO_2 oxidation, k_{SO_2} = 69 s^{-1}, and the activation energy, E_a = 63 kJ/mol [34].

As can be seen in Figure 9, compared with the reference case, the PSD of submicron particles calculated by the "adding SO_2 case" was reduced sharply, with the peak diameter being significantly reduced and the peak width being narrowed. In addition, there was also a 'shoulder peak' near 1 μm, indicating that the mass PSDs of submicron particles were significantly reduced, and a large number of alkali vapors migrated to the vicinity of 1 μm. Since the sulfate vapor generated from sulfation was transformed into submicron particles through homogeneous nucleation, due to the lower sulfate formation, the formed particles were small in size but large in number. Alkali chloride vapor can only be transformed into particulate matter by heterogeneous condensation, which has little effect on the growth of

submicron particles. Submicron particles collide more with finer fly ash particles, combined with chloride condensation, resulting in more particles near 1 μm. It can be seen that the sulfate reaction can convert corrosive chlorides into low corrosive sulfate particles but generates much larger PM_1. Therefore, the sulfate reaction can reduce Cl corrosion rather than ash deposition.

4. Conclusions

The present work mainly developed a mathematical model based on the plug flow model and the fragmentation-coalescence mechanism to describe the behavior and evolution of ash formation and the influence of the biomass feeding rate and the flue gas cooling rate on ash properties, such as mass concentration and yields of PM_{10} and its ash elements (Na, K, and Cl) during pulverized biomass combustion, which was validated by the literature data. The model considered homogeneous nucleation of the alkali vapors, heterogeneous condensation of the vapors on newly formed particles and fly ash particles, and collision-coagulation between aerosol particles. The model was also applied to numerically study and analyze the ash formation characteristics during the cases of practical PF boiler combustion and SO_2 sulfation.

The numerical studies showed that the model can reasonably describe the ash formation process and characteristics of pulverized biomass combustion, and the influence of the biomass feeding rate and the flue gas cooling rate on the mass PSDs of PM_{10} and its elements. The model could predict that with the decrease of the cooling rate, the PSDs of PM_{10} and its elements' (Na, K, and Cl) fine-mode particles gradually moved to the large size direction, and the peak width became narrow, but the peak value slightly increased. The initial nucleation temperature and initial nucleation particle size increased with the biomass feeding rate. A high cooling rate will promote the generation of particles with a larger number but a smaller diameter. Elements Na, K, and Cl are mainly concentrated in PM_1, but rarely distributed in $PM_{1–10}$. The condensation amounts of Na, K, and Cl on coarse particles increased with the biomass feeding rate and decreased with the cooling rate. Compared to the reference case, the mass PSDs of PM_{10} calculated under the practical PF boiler combustion case moved to the larger direction as a whole and formed a "shoulder peak" near 1 μm, indicating that the ash formation characteristics obtained from in the experiment condition with the ultra-high flue gas cooling rate and minimum biomass mass may have a large deviation from that of practical biomass combustion. The result of the adding SO_2 case showed that the sulfate reaction resulted in a lower number and smaller size of submicron particles but formed a new 'shoulder peak' near 1 μm, indicating that the sulfate reaction can convert corrosive chloride into low corrosive sulfate particles, but generate a larger number of PM_1, which indicates that it can reduce Cl corrosion rather than ash deposition.

Author Contributions: Conceptualization, M.X.; methodology, M.X.; software, M.X.; validation, M.X.; investigation, M.X.; data curation, M.X.; writing—original draft preparation, M.X.; writing—review and editing, M.X. and C.S.; supervision, C.S. All authors have read and agreed to the published version of the manuscript.

Funding: This research received no external funding.

Institutional Review Board Statement: Not applicable.

Informed Consent Statement: Not applicable.

Data Availability Statement: Not applicable.

Conflicts of Interest: The authors declare no conflict of interest.

Nomenclature

R_x	the percentage of the sieved mass with the size larger than d_p
d_p	diameter of fuel particle, μm
λ_{fuel}	the parameter to characterize the fineness of the fuel particles, μm
n_{fuel}	the index to define the uniformity of the fuel particle sizes
$d_{p,ash}$	the ash particle size, μm
ρ_{fuel}	the fuel density, kg/m^3
ρ_{ash}	the ash density, kg/m^3
m_{fuel}	the mass of a single fuel particle, kg
m_{ash}	the mass of a single ash particle, kg
w_{ash}	the ash content of the biomass
w_{vap}	the mass fraction of the ash released into gas phase
$Kmean$	the average breaking times
k	the breaking times of a single particle
$C(i)$	Volume fraction of matter i
C_i^*	Growth rate of the critical cluster of matter i, mol/(m^3·s)
C_k, C_i	Cunningham sliding factor of particles k and i
$d_{p,ex}$	the diameter of an existing particle, μm
D	Gas molecular diffusion rate, m^2/s
$F(Kn)$	Coefficient of correction
k_B	Boltzmann constant, 1.3806 × 10^{-23} J/K
Kn	Knudsen number
M_i	Molecular mass of matter i, kg
N_A	Avogadro constant, 6.022 × 1026/mol
N_i^e	Equilibrium concentration of critical clusters, 1/m^3
P_i	Vapor pressure of species i, Pa
P_i^s	Saturated vapor pressure of matter i, Pa
P_i^e	Vapor pressure of the vapor on the surface of the existing particles, Pa
$P_{i\infty}$	Vapor pressure on an infinite plane, Pa
R_g	Gas constant, 8.314 J/(mol·K)
S	Saturation ratio
T	Temperature, K
Z_i	Zerdovich factor
σ	Surface tension, N/m
ρ_i	Particle density of species i, kg/m^3
λ	Average free path of gas molecules, m
n_k	Number concentration of particle k, 1/m^3
$\beta_{i,k}$	Collision rate of particles (particles i and k), m^3/s
v_k, v_i	Volume of particles k and i, m^3
μ	Viscosity of medium, kg/(m·s)

References

1. Baxter, L. Biomass-coal co-combustion: Opportunity for affordable renewable energy. *Fuel* **2005**, *84*, 1295–1302. [CrossRef]
2. Livingston, W.R. *The Status of Large Scale Biomass Firing—The Milling and Combustion of Biomass Materials in Large Pulverized Coal Boilers*; IEA Bioenergy: Paris, France, 2016; p. 88; ISBN 978-1-910154-26-7.
3. Yin, C. Development in biomass preparation for suspension firing towards higher biomass shares and better boiler performance and fuel range ability. *Energy* **2020**, *196*, 117–129. [CrossRef]
4. Hansen, S.B.; Jensen, P.A.; Frandsen, F.J.; Wu, H.; Bashir, M.S.; Wadenbäck, J.; Sander, B.; Glarborg, P. Deposit probe measurements in large biomass-fired grate boilers and pulverized-fuel boilers. *Energy Fuels* **2014**, *28*, 3539–3555. [CrossRef]
5. Nielsen, H.; Frandsen, F.; Damjohansen, K.; Baxter, L.L. The implications of chlorine-associated corrosion on the operation of biomass-fired boilers. *Prog. Energy Combust. Sci.* **2000**, *26*, 283–298. [CrossRef]
6. Zheng, Y.; Jensen, A.D.; Johnsson, J.E. Deactivation of V_2O_5-WO_3-TiO_2 SCR catalyst at a biomass-fired combined heat and power plant. *Appl. Catal. B Environ.* **2005**, *60*, 253–264. [CrossRef]
7. Schill, L.; Fehrmann, R. Strategies of coping with deactivation of NH_3-SCR catalysts due to biomass firing. *Catalysts* **2018**, *8*, 135. [CrossRef]
8. Olsen, B.K.; Kügler, F.; Castellino, F.; Jensen, A.D. Poisoning of vanadia based SCR catalysts by potassium: Influence of catalyst composition and potassium mobility. *Catal. Sci. Technol.* **2016**, *6*, 2249–2260. [CrossRef]

9. Nielsen, L.B.; Livbjerg, H. Combustion Aerosols from Potassium-Containing Fuels. Ph.D. Thesis, Technical University of Denmark (DTU), Lyngby, Denmark, 1998.
10. Wang, X.; Hu, Z.; Adeosun, A.; Liu, B.; Ruan, R.; Li, S.; Tan, H. Particulate matter emission and K/S/Cl transformation during biomass combustion in an entrained flow reactor. *J. Energy Inst.* **2018**, *91*, 835–844. [CrossRef]
11. Damoe, A.J.; Wu, H.; Frandsen, F.J.; Glarborg, P.; Sander, B. Impact of coal fly ash addition on combustion aerosols ($PM_{2.5}$) from full-scale suspension-firing of pulverized wood. *Energy Fuels* **2014**, *28*, 3217–3223. [CrossRef]
12. Jiang, L.; Sheng, C. Correlation of sub-micrometer ash formation from pulverized biomass combustion with ash composition. *Energy Fuels* **2019**, *33*, 5893–5902. [CrossRef]
13. Wang, Y.; Li, X.; Wendt, J.O.L. On ash deposition rates from air and oxy-combustion of pulverized coal pretroleum coke and biomass. *Energy Fuels* **2019**, *33*, 5849–5858. [CrossRef]
14. Xu, M.; Yu, D.; Yao, H.; Liu, X.; Qiao, Y. Coal combustion-generated aerosols: Formation and properties. *Proc. Combust. Inst.* **2011**, *33*, 1681–1697. [CrossRef]
15. Liaw, S.B.; Wu, H. Importance of flue gas cooling conditions in particulate matter formation during biomass combustion under conditions pertinent to pulverized fuel applications. *Proc. Combust. Inst.* **2021**, *38*, 5201–5208. [CrossRef]
16. Gao, X.; Wu, H. Combustion of volatiles produced in situ from the fast pyrolysis of woody biomass: Direct evidence on its substantial contribution to sub-micrometer particle (PM_1) emission. *Energy Fuels* **2011**, *25*, 4172–4181. [CrossRef]
17. Liaw, S.B.; Deng, C.; Wu, H. A novel two-stage alumina reactor system for burning volatiles generated in situ from biosolid: Effect of pyrolysis temperature and combustion conditions on PM_1 emission. *Energy Fuels* **2018**, *32*, 9438–9447. [CrossRef]
18. Gao, X.; Wu, H. Biochar as a fuel: 4. Emission behavior and characteristics of PM_1 and PM_{10} from the combustion of pulverized biochar in a drop-tube furnace. *Energy Fuels* **2011**, *25*, 2702–2710. [CrossRef]
19. Christensen, K.A.; Stenholm, M.; Livbjerg, H. The formation of submicron aerosol particles, HCl and SO_2 in straw-fired boilers. *J. Aerosol Sci.* **1998**, *29*, 421–444. [CrossRef]
20. Jöller, M.; Brunner, T.; Obernberger, I. Modeling of aerosol formation during biomass combustion for various furnace and boiler types. *Fuel Process. Technol.* **2007**, *88*, 1136–1147. [CrossRef]
21. Christensen, K.A.; Livbjerg, H. A plug flow model for chemical reactions and aerosol nucleation and growth in an alkali-containing flue gas. *Aerosol Sci. Technol.* **2000**, *33*, 470–489. [CrossRef]
22. Haykiri-Acma, H.; Baykan, A.; Yaman, S.; Kucukbayrak, S. Effects of fragmentation and particle size on the fuel properties of hazelnut shells. *Fuel* **2013**, *112*, 326–330. [CrossRef]
23. Hansen, S.B.; Glarborg, P.; Jappe Frandsen, F.; Jensen, P.A. Model for Deposition Build-Up in Biomass Boilers. Ph.D. Thesis, Technical University of Denmark, Lyngby, Denmark, 2015.
24. Kassman, H.; Bäfver, L.; Åmand, L. The importance of SO_2 and SO_3 for sulphation of gaseous KCl—An experimental investigation in a biomass fired CFB boiler. *Combust. Flame* **2010**, *157*, 1649–1657. [CrossRef]
25. Wu, H.; Bashir, M.S.; Jensen, P.A.; Sander, B.; Glarborg, P. Impact of coal fly ash addition on ash transformation and deposition in a full-scale wood suspension-firing boiler. *Fuel* **2013**, *113*, 632–643. [CrossRef]
26. Xu, M.; Yue, A.; Sheng, C. Modeling K-containing vapors transforming into sub-micrometer particles in flue gas of pulverized straw combustion. *Energy Fuels* **2020**, *34*, 440–449. [CrossRef]
27. Jensen, J.R.; Nielsen, L.B.; Schultz-Møller, C.; Wedel, S.; Livbjerg, H. The nucleation of aerosols in flue gases with a high content of alkali—A laboratory study. *Aerosol Sci. Technol.* **2000**, *33*, 490–509. [CrossRef]
28. Xu, M.; Sheng, C. Modelling particle size distribution of residual fly ash from pulverized biomass combustion. *J. Biobased Mater. Bioenergy* **2021**, *15*, 75–82. [CrossRef]
29. Korbee, R.; Shah, K.V.; Cieplik, M.K.; Betrand, C.I.; Vuthaluru, H.B.; van de Kamp, W.L. First line ash transformations of coal and biomass fuels during PF combustion. *Energy Fuels* **2010**, *24*, 897–909. [CrossRef]
30. Frandsen, F.J. Ash Formation, Deposition and Corrosion When Utilizing Straw for Heat and Power Production. Ph.D. Thesis, Technical University of Denmark, Kongens Lyngby, Denmark, 2011.
31. Biagini, E.; Narducci, P.; Tognotti, L. Size and structural characterization of lignin-cellulosic fuels after the rapid devolatilization. *Fuel* **2008**, *87*, 177–186. [CrossRef]
32. Holmgren, P.; Wagner, D.R.; Strandberg, A.; Molinder, R.; Wiinikka, H.; Umeki, K.; Broström, M. Size, shape, and density changes of biomass particles during rapid devolatilization. *Fuel* **2017**, *206*, 342–351. [CrossRef]
33. Rosendahl, L.A.; Yin, C.; Kær, S.K.; Friborg, K.; Overgaard, P. Physical characterization of biomass fuels prepared for suspension firing in utility boilers for CFD modelling. *Biomass Bioenergy* **2007**, *31*, 318–325. [CrossRef]
34. Zeuthen, F.J.; Livbjerg, H.; Glarborg, P.; Jappe Frandsen, F. The Formation of Aerosol Particles during Combustion of Biomass and Waste. Ph.D. Thesis, Technical University of Denmark, Lyngby, Denmark, 2007.
35. Seinfeld, J.H.; Prandis, S.N. *Atmospheric Chemistry and Physics of Air Pollution: From Air Pollution to Climate Change*, 2nd ed.; John Wiley & Sons: New York, NY, USA, 2006; pp. 491–505.
36. Hu, Z.; Wang, X.; Ruan, R.; Li, S.; Bai, S.; Zhang, J.; Tan, H. Effect of SO_2 addition on PM Formation From Biomass Combustion In An Entrained Flow Reactor. *Energy Fuels* **2018**, *32*, 11030–11037. [CrossRef]
37. Dahneke, B. *Simple Kinetic Theory of Brownian Diffusion in Vapors and Aerosols*; Meyer, R.E., Ed.; Academic Press: New York, NY, USA, 1983; pp. 97–138.

38. Allen, M.D.; Raabe, O. Slip correction measurements of spherical solid aerosol particles in an improved Millikan apparatus. *Aerosol Sci. Technol.* **1985**, *4*, 269–286. [CrossRef]
39. Jöller, M.; Brunner, T.; Obernberger, I. Modeling of aerosol formation during biomass combustion in grate furnaces and comparison with measurements. *Energy Fuels* **2005**, *19*, 311–323. [CrossRef]
40. Damoe, A.J.; Jensen, P.A.; Frandsen, F.J.; Wu, H.; Glarborg, P. Fly ash formation during suspension firing of biomass: Effects of residence time and fuel type. *Energy Fuels* **2017**, *31*, 555–570. [CrossRef]